chemengineering

MDPI

Communication

Synthesis of $ZnS/Al_2O_3/TaSe_2$ Core/Shell Nanowires Using Thin Ta Metal Film Precursor

Boris Polyakov [1,*], Kevon Kadiwala [1], Edgars Butanovs [1,2], Luize Dipane [1], Annamarija Trausa [1], Dmitry Bocharov [1,*] and Sergei Vlassov [3]

[1] Institute of Solid State Physics, University of Latvia, 8 Kengaraga Str., LV-1063 Riga, Latvia; kevon.kadiwala@cfi.lu.lv (K.K.); edgars.butanovs@cfi.lu.lv (E.B.); luize.dipane@cfi.lu.lv (L.D.); annamarija.trausa@cfi.lu.lv (A.T.)
[2] Institute of Technology, University of Tartu, Nooruse 1, 50411 Tartu, Estonia
[3] Institute of Physics, University of Tartu, W. Ostwaldi Str. 1, 50412 Tartu, Estonia; sergei.vlassov@ut.ee
* Correspondence: boris.polyakov@cfi.lu.lv (B.P.); bocharov@cfi.lu.lv (D.B.)

Abstract: This study introduces a novel approach for fabricating $ZnS/Al_2O_3/TaSe_2$ heterostructured core/shell nanowires (NWs) through the selenization of a metallic Ta thin film precursor. The synthesis process involves a meticulously designed four-step protocol: (1) generating ZnS NWs on an oxidized silicon substrate, (2) encapsulating these NWs with a precisely controlled thin Al_2O_3 layer via atomic layer deposition (ALD), (3) applying a Ta precursor layer by magnetron sputtering, and (4) annealing in a Se-rich environment in a vacuum-sealed quartz ampoule to transform the Ta layer into $TaSe_2$, resulting in the final core/shell structure. The characterization of the newly produced NWs using scanning electron microscopy (SEM), transmission electron microscopy (TEM), X-ray diffraction (XRD), and X-ray photoelectron spectroscopy (XPS) was validated using the integrity and composition of the heterostructures. Our method not only establishes a new pathway for the synthesis of $TaSe_2$-based core/shell NWs but also extends the potential for creating a variety of core/shell NW systems with chalcogenide shells by adapting the thin film metal precursor approach. This versatility opens the way for future advancements in nanoscale material applications, particularly in electronics and optoelectronics where core/shell geometries are increasingly important.

Keywords: heterogeneous 1D nanostructures; transition metal dichalcogenides; vapour liquid solid method; atomic layer deposition; magnetron sputtering; selenization

Citation: Polyakov, B.; Kadiwala, K.; Butanovs, E.; Dipane, L.; Trausa, A.; Bocharov, D.; Vlassov, S. Synthesis of $ZnS/Al_2O_3/TaSe_2$ Core/Shell Nanowires Using Thin Ta Metal Film Precursor. *ChemEngineering* **2024**, *8*, 25. https://doi.org/10.3390/chemengineering8010025

Received: 9 November 2023
Revised: 22 January 2024
Accepted: 11 February 2024
Published: 19 February 2024

1. Introduction

In the last decade, layered two-dimensional (2D) chalcogenide materials, transition metal dichalcogenides (TMDs) in particular, have attracted significant attention in the material science research community [1–7]. Layered or van der Waals transition metal dichalcogenides (TMDs), and characterized by the general formula MX_2 (where 'M' includes metals such as V, Mo, Hf, Ta, W, and Re among others, and 'X' stands for S, Se, and Te), they demonstrate semiconducting or metallic properties [8,9]. $TaSe_2$ polymorphs are a typical layered TMD material belonging to the hexagonal crystal family that exhibits multiple charge density wave (CDW) phase transitions [9]. $TaSe_2$ can exist in several polytypes: the 1T, 2H, and 3R [10] as well as 4Hb [11] structures, each with distinct symmetry and physical properties. 1T-$TaSe_2$ has a trigonal D_{3d} symmetry (space-group Nr. 164 or $P\bar{3}m1$), where each Ta atom is octahedrally coordinated by six Se atoms [10]. 2H-$TaSe_2$ and related 4Hb-$TaSe_2$, which are minimally different due to the relative shift of layers relative to each other, are more stable phases and have a D_{6h} symmetry (space-group Nr. 194 or $P6_3/mmc$), where each Ta atom is coordinated by six Se atoms in a trigonal prismatic arrangement [10]. The structure of the atomic environment of Ta atoms in 1T-$TaSe_2$ and 2H-$TaSe_2$ phases is shown in the picture (Figure S1). 1T-$TaSe_2$ is a metal with lattice parameters of a = 0.348 nm

and c = 0.627 nm [12], while 2H-$TaSe_2$ and 4Hb-$TaSe_2$ are semiconductors with lattice parameters of a = 0.343 nm and c = 1.27 nm [13] and of a = 0.3455 nm and c = 2.5148 nm [11] for 2H-$TaSe_2$ and 4Hb-$TaSe_2$ phases, respectively.

Core-shell based designs featuring core-shell nanowires (NW) and including 1D/2D heterostructures, such as 1D NWs coated with 2D layered materials, are highly promising in various applications for harvesting solar energy [14]. These 1D/2D heterostructures also demonstrate aptness for use in photocatalytic processes, notably in the hydrogen evolution reaction [15,16]. Furthermore, they possess advantageous optical properties, such as improved photoelectric efficiency [17], rendering them potentially effective for use in imaging and sensing technologies [18]. Additionally, 1D/2D heterostructures can be used as a template for thin 2D materials, which bring mechanical stability to 2D materials and help to anchor 2D structures to the substrate. Thin, free-standing 2D materials are very soft and cannot be manipulated without a stiff substrate or template [19]. Moreover, combining layered two-dimensional materials with semiconducting nanowires facilitates the development of sophisticated core/shell heterostructures with enhanced optoelectronic properties, e.g., greatly increased photosensitivity and a faster photoresponse time [18].

It is worth noting that, at high temperatures in a corrosive atmosphere, (S, Se) ZnO NWs are insufficiently chemically stable, and the use of ZnS NWs is preferable.

ZnS is a direct bandgap semiconductor with two polytypes: the most stable zincblende (or sphalerite) cubic diamond-like phase (space group Nr. 216 or $F\bar{4}3m$) with a bandgap of 3.6 eV, and high-temperature hexagonal wurtzite phase (space group Nr. 186 or $P6_3mc$) with bandgap 3.9 eV (visual representation of crystal structure for both ZnS phases is shown in Figure S1a) [20]. For both compounds, zinc and sulfur are tetrahedrally coordinated. ZnS is nontoxic, environmentally friendly, and a low-cost compound made of earth-abundant elements. Zinc sulfide demonstrates transparency across a broad spectrum of wavelengths. This characteristic renders it highly suitable for use in electroluminescent devices [21]. Additionally, its properties are advantageous for a variety of applications in electronics, optoelectronics, and sensors [22].

A thin layer of Al_2O_3 can be precisely deposited by atomic layer deposition (ALD) with sub-angstrom accuracy [23,24]. It was demonstrated that a thin layer of amorphous Al_2O_3 deposited by ALD around NWs helps to protect the core material from fracture and allows it to withstand significantly higher deformations and stresses in comparison to uncoated NW [25]. Moreover, an Al_2O_3 layer is able to preserve core NWs morphology in a corrosive chalcogenide atmosphere at elevated temperatures and facilitate the smooth growth of TMDs shell around NWs [26].

Thin films or even monolayers of $TaSe_2$ can be grown by chemical vapor deposition (CVD) methods. For example, Shi et al. [27] demonstrated the growth of wafer-scale uniform monolayer 2H-$TaSe_2$ films on Au foil from $TaCl_5$ and selenium precursors at 930 °C in a mixed Ar/H_2 gas flow. It is important to note that the $TaCl_5$ precursor is atmosphere-sensitive and requires manipulation in an inert atmosphere (glovebox). An alternative method of Ta deposition for fabrication of core-shell nanostructures is based on the anodization process reported by Pligovka et al. [28]. Wang et al. reported the synthesis of 1T-$TaSe_2$ on a Si/SiO_2 substrate using $Ta_2O_5/MgCl_2$ selenium in a temperature range from 640 to 890 °C in a mixed Ar/H_2 gas flow [12]. For the synthesis of 1D core/shell nanostructures, the direct deposition of transition metal oxide WO_3, MoO_3, and ReO_3 precursors can be used, as was shown in [18,26,29]. However, in contrast to these transition metal oxides that have medium-high sublimation/melting temperatures in the range 500–750 °C [30,31], tantalum oxide Ta_2O_5 has a very high melting point of 1872 °C and high chemical stability [30]. The chalcogenization of Ta_2O_5 requires a rather long processing time due to the high chemical stability of tantalum pentoxide. For example, Li et al. produced TaS_2 nanotubes by the sulfurization of Ta_2O_5 nanotubes at 625 °C under H_2S gas flow during a 24 h long process [32].

Both TaS_2 and $TaSe_2$ nanomaterials are expected to be effective catalysts for the hydrogen evolution reaction (HER) [33–35]; however, the controllable fabrication of 1D arrays of

$TaSe_2$ and TaS_2 nanostructures still remains challenging and slows down the progress on their possible applications in catalysis and HER.

This study reports the synthesis of $ZnS/Al_2O_3/TaSe_2$ core/shell NWs using their ZnS/Al_2O_3 NWs as a template. As an alternative Ta-based TMD precursor, a thin metallic Ta film is proposed, which can be deposited by magnetron sputtering and subsequently selenized at medium-high temperatures of 650–750 ºC in a vacuum-sealed quartz ampoule using a Se precursor. The magnetron deposition of thin films is a scalable technology, which allows a significant decrease in the consumption of Ta and makes it more ecologically friendly. The approach described in the present work can be used for the synthesis of other core/shell NWs with a layered 2D chalcogenides shell (such as selenides and sulfides), using appropriate metal precursors, including those of other transition metals.

2. Experimental Details

2.1. Materials and Methods

The fabrication of $ZnS/Al_2O_3/TaSe_2$ core/shell NWs was accomplished using a four-step method (see Figure 1):

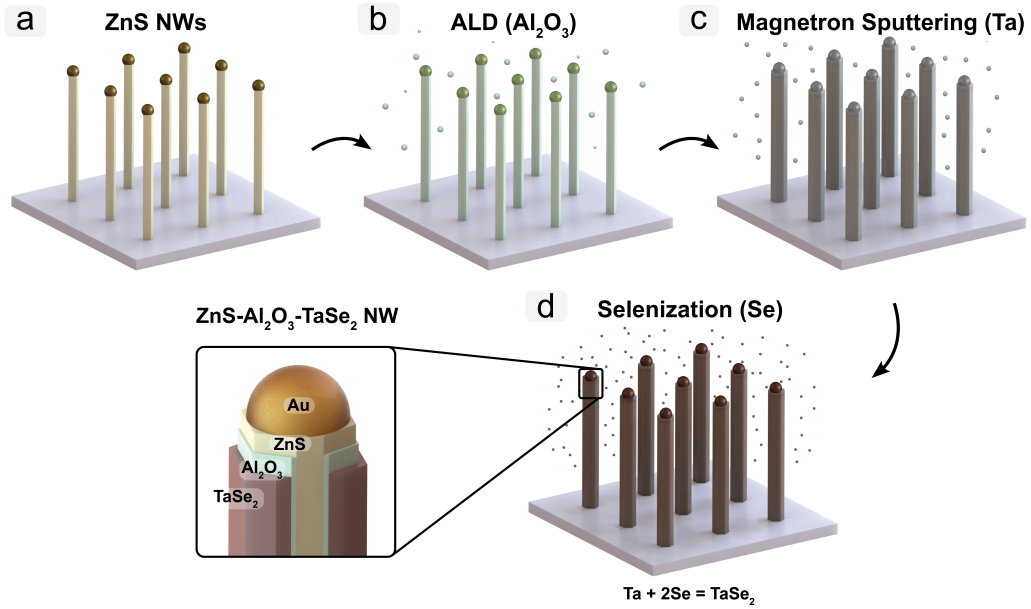

Figure 1. A scheme for the four-step method for the fabrication of $ZnS/Al_2O_3/TaSe_2$ core/shell NWs. Growth of ZnS NWs via VLS mechanism using Au NPs catalysts (**a**). Al_2O_3 layer deposition by ALD around ZnS NWs (**b**). Ta thin film deposition on ZnS/Al_2O_3 NWs (**c**). Selenization of Ta thin film and formation of NWs $ZnS/Al_2O_3/TaSe_2$ NWs (**d**).

1. In the initial step, ZnS NWs were synthesized on top of the oxidized silicon wafers Si/SiO_2 (Si(100) wafer, 50 nm of thermal oxide, Semiconductor Wafer, Inc., Hsinchu, Taiwan) using the Au nanoparticles (50 nm in diameter, water suspension, BBI International, Grand Forks, ND, USA) as a catalyst for vapor–liquid–solid (VLS) growth. ZnS powder 0.4 g (>97%, Sigma Aldrich, St. Louis, MO, USA) was thermally sublimated in a quartz tube reactor at a temperature of 950 °C for 30 min, followed by natural cooling. The ZnS vapor was carried downstream by a Ar/H_2 35% gas mixture to the substrate to grow ZnS NWs.
2. Subsequently, a thin Al_2O_3 layer was deposited on the NWs using the ALD technique in a Savannah S100 reactor. The deposition process, carried out at 150 °C, involved 66 cycles (Al_2O_3 thickness ~6 nm) of alternating Trimethylaluminum (TMA) and H_2O as precursors, with N_2 serving as the inert carrier gas.
3. A Ta metallic layer, approximately 15 nm thick on flat substrates, was deposited over the ZnS/Al_2O_3 NWs using direct current (DC) magnetron sputtering from a Ta target

in an Ar atmosphere (4×10^{-3} torr, 30 sccm Ar gas flow at 100 W DC power). It is noteworthy that, due to geometrical factors, the actual thickness of the Ta film on the vertical NWs might be less than 15 nm.

4. The final step was the annealing of the coated NWs in a selenium environment. The samples underwent a 50-min anneal at 650 °C within a vacuum-sealed quartz ampoule to transform the metallic Ta layer into $TaSe_2$. The procedure involved placing the Si/SiO_2 wafer with ZnS/Al_2O_3/Ta NWs or a Ta thin film on Si/SiO_2 inside the ampoule, which was then evacuated using a turbo pump (vacuum better than 10^{-3} torr) and hermetically sealed. Selenium pellets (50 mg, Sigma Aldrich) and Ta foil (100 mg, GoodFellow, Huntingdon, UK) were also introduced into the ampoule to maintain a stable vapor pressure of $TaSe_2$ and to minimize the vapor's transport to cooler areas of the ampoule. The length of ampoule was tailored to align with the hot zone of the oven, ensuring that its ends remained cooler, which, in turn, allowed for the condensation of any unreacted selenium (Figure S2, Supplementary data).

2.2. Characterisation

The phase composition of the samples was determined through X-ray diffraction (XRD), conducted on a Rigaku MiniFlex 600 X-ray powder diffractometer. This equipment employs Bragg–Brentano θ–2θ geometry and is equipped with a 600 W Cu anode, utilizing Cu Kα radiation ($\lambda = 1.5406$ Å). Rietveld Analysis was performed using the BGMN program with a graphical user interface Profex [36]. For verifying the chemical composition of the NW samples, X-ray photoelectron spectroscopy (XPS) was conducted using an ESCALAB Xi spectrometer from ThermoFisher. The excitation source was an Al Kα X-ray tube, operating at an energy of 1486 eV. The examination area of the samples measured 650 µm × 100 µm, and the sample surface was positioned at a 90° angle to the analyzer. Sputter-cleaning before the measurements was not used. An electron gun was used to perform charge compensation. The base pressure during the spectra acquisition was better than 10^{-5} Pa.

The internal crystalline structure of core/shell NWs, placed on a Lacey Cu Transmission Electron Microscope grid (Agar Scientific, Essex, UK), was examined using a Transmission Electron Microscope (Tecnai GF20, FEI, Hillsboro, OR, USA) functioning at an acceleration voltage of 200 kV. To analyze the morphology of these core/shell NWs, scanning electron microscopy (SEM, Lyra, Tescan, Brno, Czech Republic) was employed at an accelerating voltage of 12 keV, complemented by high-resolution SEM at 5 keV using a Helios 5 UX (Thermo Fisher Instruments, Waltham, MA, USA).

3. Results and Discussion

The phase composition of the selenized ZnS/Al_2O_3/Ta NWs on oxidized Si/SiO_2 substrates was studied by XRD using the Rietveld method, and the result of the refinement is shown in Figure 2. The main 4Hb-$TaSe_2$ characteristic peak (004) was identified [11], confirming the successful selenization of the Ta coating. The wurtzite ZnS phase ([37] and ICDD 36-1450 [38]) for the NWs' core was also detected [39]. It is important to note that no ZnSe peaks can be seen in the XRD pattern, which means the selenization of the ZnS NWs core did not occur. On the other hand, a β-Ta_2O_5 (space group Nr. 49 or Pccm and lattice parameters of $a = 0.6217$, $b = 0.3677$ and $c = 0.7794$ nm [40,41]) (001) peak was detected, possibly due to some oxidation of the Ta coating when exposed to air and subsequent crystallization during high-temperature processing in the ampoule [42]. Nonetheless, no peaks corresponding to Al_2O_3 were detected, likely due to the amorphous nature and high crystallization temperature of the ALD coating. Additional Bragg peaks identified in the XRD patterns were ascribed to the Si(100) substrate (the forbidden Si(200) reflection at $2\theta \approx 33°$), and the gold (ICDD 04-0784 [43,44]) nanoparticles employed in the VLS growth process. Crystallographic data for Rietveld analysis taken from refs. [11,37,40,44] were used for 4Hb-$TaSe_2$, Zn, Ta_2O_5, and Au, respectively.

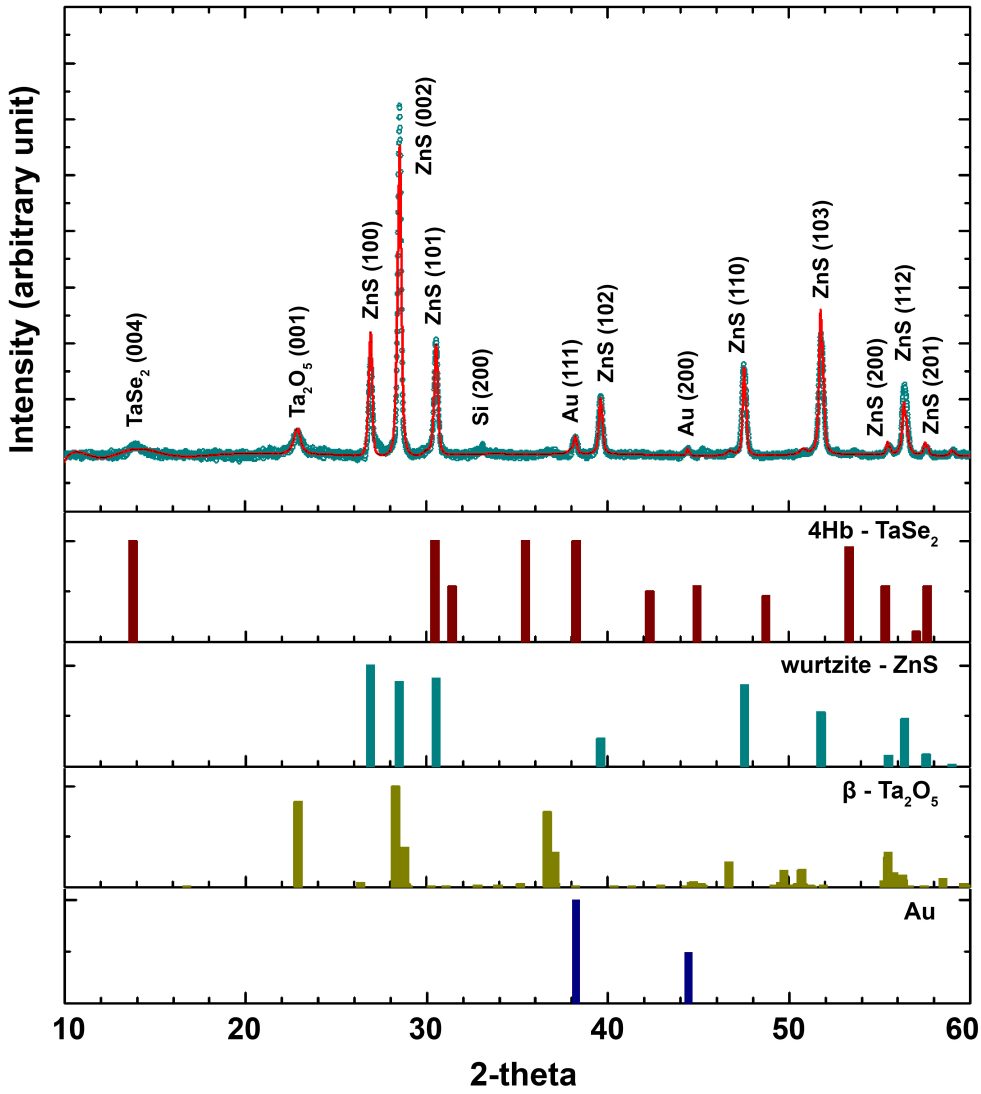

Figure 2. Rietveld refinement (solid line) of the X-ray diffraction pattern (open circles) for selenized $ZnS/Al_2O_3/Ta$ NWs on an oxidized Si/SiO_2 substrate. The corresponding Bragg indexes for each crystalline phase have been identified and marked, as well as XRD patterns for 4Hb-$TaSe_2$ [11], wurtzite ZnS phase [37], β-Ta_2O_5 [40] and Au [44].

XPS analysis further validated the chemical states within the shell of the heterostructured NWs, as depicted in Figure 3 (survey scan presented in Figure S3). High-resolution spectra of the Ta 4f and Se 3d peaks were acquired and calibrated relative to the adventitious C 1s peak at 284.8 eV. No other elements, except the constituents of the SiO_2 substrate, were detected due to the tantalum selenide coating and carbon layer. A Ta 4f scan revealed a peak consisting of two doublets. To mitigate the error during the peak fitting, a spin-orbit splitting $\Delta_{7/2-5/2} = 1.91$ eV was fixed between the Ta $4f_{7/2}$ and $4f_{5/2}$ components in each doublet and the area ratio was held at 4:3. The first doublet with a Ta $4f_{7/2}$ peak at 25.2 eV corresponded well to the Ta valence state 4^+ in the $TaSe_2$ compound [27,45]. The other Ta $4f_{7/2}$ peak, shifted to higher energies at 27.0 eV, was attributed to the Ta chemical state with valence 5^+ [27,42], as in the Ta_2O_5 compound. The presence of the β-Ta_2O_5 phase was also confirmed by the XRD measurements. $TaSe_2$ is known to be susceptible to oxidation in ambient conditions, especially in its nanostructured form, thus the material should be handled and stored in an oxygen-free environment to increase its stability. The Se $3d_{5/2}$ peak was located at 55.6 eV (spin-orbit splitting $\Delta_{5/2-3/2} = 0.86$ eV), matching tantalum selenide [45].

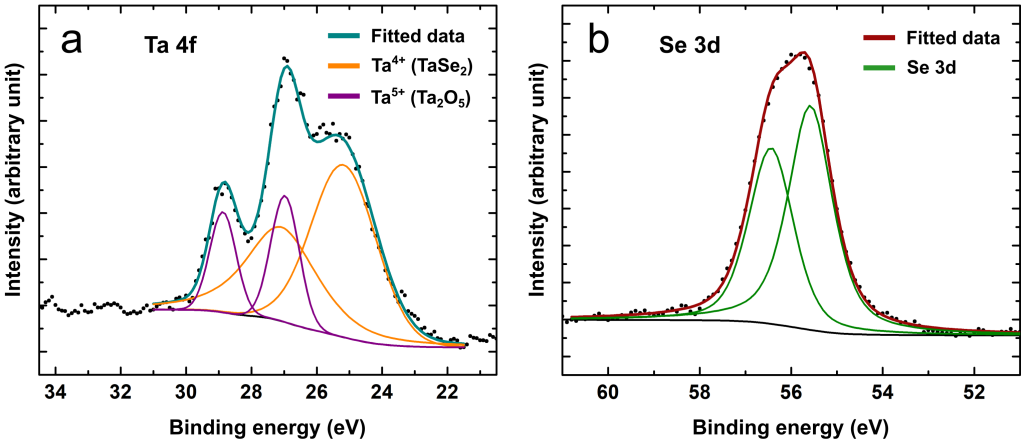

Figure 3. High-resolution XPS spectra of the selenized ZnS/Al_2O_3/Ta NWs elements for (**a**) Ta and (**b**) Se. Ta 4f peak scan fitting revealed two chemical states (Ta 4^+ and 5^+) present in the sample.

To determine the geometry and morphology of the core/shell NWs, SEM was used (Figure 4). According to the SEM images, NWs have a straight shape and a length in the order of 10 microns. The preservation of the straight shape of NWs is important because the shape and integrity of NWs can be compromised at high temperatures and in an aggressive corrosive atmosphere. As mentioned before, a thin layer of Al_2O_3 was used to cover and protect NWs during the selenization procedure, similar to in our previous work [26].

TEM microscopy was used to investigate the morphology and inner structure of core/shell NWs in detail. Typical images of two core/shell NW are presented in Figure 5. At the ends of every NW, Au nanoparticles can be seen, which is typical for the VLS growth mechanism. Au NPs appear as bright dots in the SEM images (Figure 4b) and as black dots in the TEM images (Figure 5a,b). Upon the selenization of the Ta shell, a TMD layer of $TaSe_2$ can be seen around NWs, which appears as black parallel lines (Figure 5b). The shell thickness varies from ~10 layers to ~20, with interlayer distance measured around 0.627 nm, which corresponds very well to the 0.627 nm interlayer distance in the 1T-$TaSe_2$ [12], 0.635 nm in the 2H-$TaSe_2$ [13], and 0.6287 in the 4Hb-$TaSe_2$ [11] materials. A layer of non-crystalline carbon was discovered atop the $TaSe_2$ surface, potentially formed through catalysis from carbon present in the atmosphere. More TEM images of selenized ZnS/Al_2O_3/Ta NWs can be found in Figure S3 in the Supplementary Data file. It was impossible to achieve the atomic resolution of the Al_2O_3 interlayer, which covers ZnS NWs; however, the thickness of the amorphous spacing between ZnS and $TaSe_2$ corresponds well to the expected Al_2O_3 thickness.

A similar approach was tested for ZnO/Al_2O_3/Ta NWs at the same temperature and selenization procedure duration. The ZnO NWs core completely sublimated during the selenization procedure; however, the Al_2O_3 shell was intact and $TaSe_2$ layer successfully produced, which can potentially be used for the preparation of hollow core tube-like Al_2O_3/$TaSe_2$ 1D heterostructures. The TEM images of the selenized ZnO/Al_2O_3/Ta NWs can be found in Figure S5 in the Supplementary Data file.

It is interesting to note that attempts to selenize Ta thin films and core-shell structures at atmospheric pressure using gas flow, all conducted at the same temperature, were unsuccessful. Additionally, the in-ampoule selenization of other metals, namely T and V, was tested within the same temperature range, yielding positive results. The vapor pressure of these refractory metals at temperatures between 650–700 °C is relatively low. This opens an additional option for the selenization of sandwich-like composite structures. However, further dedicated research is required to validate this hypothesis.

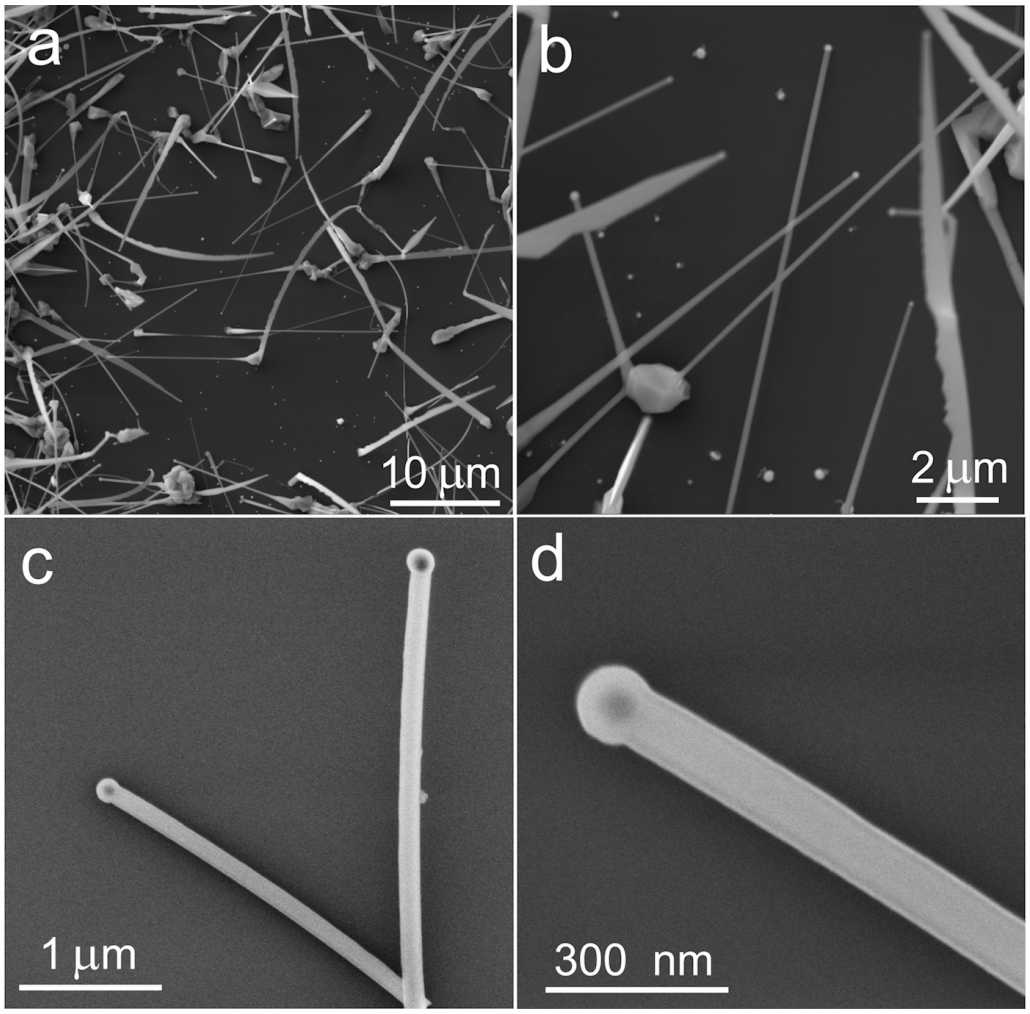

Figure 4. SEM images of selenized $ZnS/Al_2O_3/Ta$ NWs grown on Si/SiO_2 substrate at different magnifications taken at 12 keV (**a**,**b**) and 5 keV (**c**,**d**), respectively.

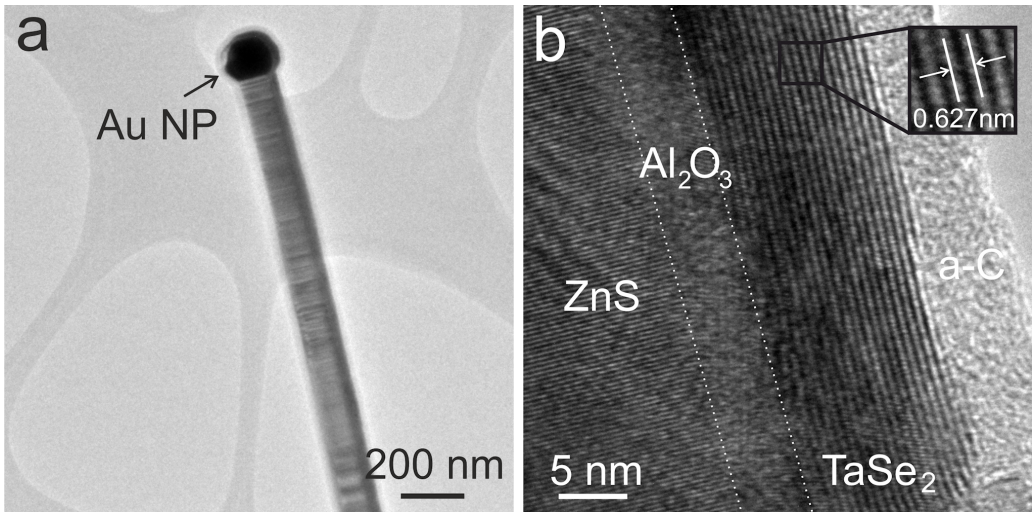

Figure 5. TEM images of $ZnS/Al_2O_3/TaSe_2$ NWs at different magnifications. A single $ZnS/Al_2O_3/TaSe_2$ NW with a Au NP at the end on a Lacey carbon-coated TEM grid (**a**). $ZnS/Al_2O_3/TaSe_2$ NW at high magnification; the individual layers of the heterostructure are identified, and amorphous carbon (a-C) is also present on top of the $TaSe_2$ shell (**b**).

4. Conclusions

This study presents the development of a robust method for fabricating core/shell NWs with a two-dimensional transition metal dichalcogenide (TMD) shell by selenizing a thin film of tantalum. The process entails a four-step synthesis routine: (1) synthesis of ZnS NWs on a silicon wafer, (2) deposition of a thin Al_2O_3 layer by atomic layer deposition (ALD), (3) magnetron sputtering of a Ta layer, and (4) annealing of the ZnS/Al_2O_3/Ta NWs in a selenium atmosphere within a vacuum-sealed quartz ampoule at 650 °C to form the core/shell structure. Through this technique, complete transformation of the metallic Ta layer into a well-defined $TaSe_2$ shell around the ZnS/Al_2O_3 NWs was achieved. Characterization of the synthesized core/shell ZnS/Al_2O_3/$TaSe_2$ NWs by XRD, XPS, TEM, and SEM confirmed the formation of the desired core/shell structure with the integrity of the NWs preserved throughout the selenization process.

The significance of this work lies in its introduction of a scalable and versatile method for fabricating core/shell NWs with 2D TMD shells based on selenization of thin metal Ta film. This technique extends beyond $TaSe_2$, applicable to a range of 2D chalcogenides, like selenides and sulfides, using various metal precursors, including Ti and other refractory metals. Such versatility in the fabrication process expands the potential for creating a diverse range of core/shell NW systems, which is crucial for advancing material applications at the nanoscale. The unique properties of 2D materials as well as the method presented in the paper open ways for future research and development in nanostructures, with potential breakthroughs in energy harvesting, sensing, and nanodevice fabrication.

Supplementary Materials: The following supporting information can be downloaded at: https://www.mdpi.com/article/10.3390/chemengineering8010025/s1, Figure S1: Visual representation of crystal structure of ZnS zincblende (a, left panel) and wurtzite (a, right panel), as well as 1T-$TaSe_2$ and 2H-$TaSe_2$ (top view in (b) and side view in (c)). Atomic environment of Se atoms around Ta is shown in (c) for better explanation. Unit cell for each structure is shown with black polyhedral. 1T-$TaSe_2$ has a trigonal D_{3d} space group symmetry, where each Ta atom is octahedrally coordinated by six Se atoms. 2H-$TaSe_2$ is a more stable phase and has a D_{6h} space-group symmetry, where each Ta atom is coordinated by six Se atoms in a trigonal prismatic arrangement. For 1T-$TaSe_2$ cells is doubled in z–direction for better comparison between both phases of $TaSe_2$; Figure S2: Selenization of Ta thin film and ZnS/Al_2O_3/$TaSe_2$ NWs on Si/SiO_2 substrate in quartz ampoule. Images before ampoule heating (a), during ampoule heating (b), during cooling (c); Figure S3: XPS survey scan for ZnS/Al_2O_3/$TaSe_2$ NWs on Si/SiO_2 substrate. The characteristic peaks of all elements present on the sample surface are marked correspondingly; Figure S4: TEM images of ZnS/Al_2O_3/$TaSe_2$ NWs at low (a,c,e) and high (b,d,f) magnifications; Figure S5: TEM images of ZnO/Al_2O_3/$TaSe_2$ NWs at low (a) and high (b) magnifications. ZnO NW core was sublimated and $TaSe_2$ shell cover Al_2O_3 empty "tube".

Author Contributions: Conceptualization, B.P.; methodology, B.P., E.B. and S.V.; validation, D.B.; investigation, B.P., K.K., E.B., L.D. and A.T.; data curation, K.K. and E.B.; formal analysis: D.B.; writing—original draft preparation, B.P.; writing—review and editing, E.B., D.B. and S.V.; visualization, K.K. and D.B.; supervision, B.P. and E.B. project administration, B.P.; funding acquisition, B.P. and D.B. All authors have read and agreed to the published version of the manuscript.

Funding: This research was funded by the Latvian Council of Science project (Nr. lzp-2020/1-0261). E.B. and S.V. were supported by the European Union's Horizon 2020 program, under Grant Agreement No. 856705 (ERA Chair "MATTER"). The Institute of Solid State Physics, University of Latvia (Latvia) as the Centre of Excellence has received funding from the European Union's Horizon 2020 Framework Programme H2020-WIDESPREAD01-2016-2017-Teaming Phase2 under grant agreement no. 739508, project CAMART^2.

Data Availability Statement: The data that support the findings of this study are available on request.

Acknowledgments: The authors thank Alexei Kuzmin very much for his kind assistance in performing the Rietveld analysis.

Conflicts of Interest: The authors declare no conflicts of interest.

References

1. Yin, X.; Tang, S.; Zheng, Y.; Gao, J.; Wu, J.; Zhang, H.; Chhowalla, M.; Chen, W.; Wee, A. Recent developments in 2D transition metal dichalcogenides: Phase transition and applications of the (quasi-)metallic phases. *Chem. Soc. Rev.* **2021**, *50*, 10087–10115. [CrossRef] [PubMed]
2. Ali, H.G.; Khan, K.; Hanif, M.; Khan, M.Z.; Hussain, I.; Javed, M.S.; AL-bonsrulah, H.A.; Mosiałek, M.; Fichtner, M.; Motola, M. Advancements in two-dimensional materials as anodes for lithium-ion batteries: Exploring composition-structure-property relationships, emerging trends, and future perspective. *J. Energy Storage* **2023**, *73*, 108980. [CrossRef]
3. Wang, Q.H.; Kalantar-Zadeh, K.; Kis, A.; Coleman, J.N.; Strano, M.S. Electronics and optoelectronics of two-dimensional transition metal dichalcogenides. *Nat. Nanotechnol.* **2012**, *7*, 699–712. [CrossRef] [PubMed]
4. Jariwala, D.; Sangwan, V.K.; Lauhon, L.J.; Marks, T.J.; Hersam, M.C. Emerging Device Applications for Semiconducting Two-Dimensional Transition Metal Dichalcogenides. *ACS Nano* **2014**, *8*, 1102–1120. [CrossRef] [PubMed]
5. Manzeli, S.; Ovchinnikov, D.; Pasquier, D.; Yazyev, O.; Kis, A. 2D transition metal dichalcogenides. *Nat. Rev. Mater.* **2017**, *2*, 17033. [CrossRef]
6. Lasek, K.; Li, J.; Kolekar, S.; Coelho, P.M.; Guo, L.; Zhang, M.; Wang, Z.; Batzill, M. Synthesis and characterization of 2D transition metal dichalcogenides: Recent progress from a vacuum surface science perspective. *Surf. Sci. Rep.* **2021**, *76*, 100523. [CrossRef]
7. Ali, S.; Ahmad Shah, S.S.; Sufyan Javed, M.; Najam, T.; Parkash, A.; Khan, S.; Bajaber, M.A.; Eldin, S.M.M.; Tayeb, R.A.; Rahman, M.M.; et al. Recent Advances of Transition Metal Dichalcogenides-Based Materials for Energy Storage Devices, in View of Monovalent to Divalent Ions. *Chem. Rec.* **2023**, *24*, e202300145. [CrossRef]
8. Choi, W.; Choudhary, N.; Han, G.; Park, J.; Akinwande, D.; Lee, Y. Recent development of two-dimensional transition metal dichalcogenides and their applications. *Mater. Today* **2017**, *20*, 116–130. [CrossRef]
9. Hossain, M.; Zhao, Z.; Wen, W.; Wang, X.; Wu, J.; Xie, L. Recent Advances in Two-Dimensional Materials with Charge Density Waves: Synthesis, Characterization and Applications. *Crystals* **2017**, *7*, 298. [CrossRef]
10. Wang, H.; Chen, Y.; Zhu, C.; Wang, X.; Zhang, H.; Tsang, S.; Li, H.; Lin, J.; Yu, T.; Liu, Z.; et al. Synthesis of Atomically Thin 1T-$TaSe_2$ with a Strongly Enhanced Charge-Density-Wave Order. *Adv. Funct. Mater.* **2020**, *30*, 2001903. [CrossRef]
11. Lüdecke, J.; van Smaalen, S.; Spijkerman, A.; de Boer, J.L.; Wiegers, G.A. Commensurately modulated structure of $4H_b$–$TaSe_2$ determined by X-ray crystal-structure refinement. *Phys. Rev. B* **1999**, *59*, 6063–6071. [CrossRef]
12. Samnakay, R.; Wickramaratne, D.; Pope, T.; Lake, R.; Salguero, T.; Balandin, A. Zone-Folded Phonons and the Commensurate–Incommensurate Charge-Density-Wave Transition in 1T-$TaSe_2$ Thin Films. *Nano Lett.* **2015**, *15*, 2965–2973. [CrossRef] [PubMed]
13. Bjerkelund, E.; Kjekshus, A. On the structural properties of the $Ta_{1+x}Se_2$. *Acta Chem. Scand.* **1967**, *21*, 513–526. [CrossRef]
14. Liu, S.; Tang, Z.R.; Sun, Y.; Colmenares, J.; Xu, Y.J. One-dimension-based spatially ordered architectures for solar energy conversion. *Chem. Soc. Rev.* **2015**, *44*, 5053–5075. [CrossRef]
15. Lin, Y.P.; Polyakov, B.; Butanovs, E.; Popov, A.; Sokolov, M.; Bocharov, D.; Piskunov, S. Excited states calculations of MoS_2@ZnO and WS_2@ZnO two-dimensional nanocomposites for water-splitting applications. *Energies* **2022**, *15*, 150. [CrossRef]
16. Liu, Y.; Xie, S.; Li, H.; Wang, X. A highly efficient sunlight driven ZnO nanosheet photocatalyst: Synergetic effect of P-doping and MoS_2 atomic layer loading. *ChemCatChem* **2014**, *6*, 2522–2526. [CrossRef]
17. Aldalbahi, A.; Wang, Z.B.; Ahamad, T.; Alshehri, S.; Feng, P. Two-step facile preparation of 2D MoS_2/ZnO nanocomposite p-n junctions with enhanced photoelectric performance. *Int. J. Photoenergy* **2021**, *2021*, e1884293. [CrossRef]
18. Butanovs, E.; Vlassov, S.; Kuzmin, A.; Piskunov, S.; Butikova, J.; Polyakov, B. Fast-response single-nanowire photodetector based on ZnO/WS_2 core/shell heterostructures. *ACS Appl. Mater. Interfaces* **2018**, *10*, 13869–13876. [CrossRef]
19. Han, S.; Meng, Y.; Xu, Z.; Kim, J.S.; Li, Y.; Roh, I.; Ahn, H.; Kim, D.; Bae, S. Freestanding Membranes for Unique Functionality in Electronics. *ACS Appl. Electron. Mater.* **2023**, *5*, 690–704. [CrossRef]
20. Ong, H.; Chang, R. Optical constants of wurtzite ZnS thin films determined by spectroscopic ellipsometry. *Appl. Phys. Lett.* **2001**, *79*, 3612–3614. [CrossRef]
21. Dimitrova, V.; Tate, J. Synthesis and characterization of some ZnS-based thin film phosphors for electroluminescent device applications. *Thin Solid Films* **2000**, *365*, 134–138. [CrossRef]
22. Fang, X.; Zhai, T.; Gautam, U.; Li, L.; Wu, L.; Bando, Y.; Golberg, D. ZnS nanostructures: From synthesis to applications. *Prog. Mater. Sci.* **2011**, *56*, 175–287. [CrossRef]
23. Sperling, B.; Kalanyan, B.; Maslar, J. Atomic Layer Deposition of Al_2O_3 Using Trimethylaluminum and H_2O: The Kinetics of the H_2O Half-Cycle. *J. Phys. Chem. C* **2020**, *124*, 3410–3420. [CrossRef]
24. Prokes, S.; Katz, M.; Twigg, M. Growth of crystalline Al_2O_3 via thermal atomic layer deposition: Nanomaterial phase stabilization. *APL Mater.* **2014**, *2*, 032105. [CrossRef]
25. Vlassov, S.; Polyakov, B.; Vahtrus, M.; Mets, M.; Antsov, M.; Oras, S.; Tarre, A.; Arroval, T.; Lohmus, R.; Aarik, J. Enhanced flexibility and electron-beam-controlled shape recovery in alumina-coated Au and Ag core-shell nanowires. *Nanotechnology* **2017**, *28*, 505707. [CrossRef] [PubMed]
26. Butanovs, E.; Kuzmin, A.; Zolotarjovs, A.; Vlassov, S.; Polyakov, B. The role of Al_2O_3 interlayer in the synthesis of ZnS/Al_2O_3/MoS_2 core-shell nanowires. *J. Alloys Compd.* **2022**, 165648. [CrossRef]
27. Shi, J.; Chen, X.; Zhao, L.; Gong, Y.; Hong, M.; Huan, Y.; Zhang, Z.; Yang, P.; Li, Y.; Zhang, Q.; et al. Chemical Vapor Deposition Grown Wafer-Scale 2D Tantalum Diselenide with Robust Charge-Density-Wave Order. *Adv. Mater.* **2018**, *30*, 1804616. [CrossRef]

28. Pligovka, A.; Lazavenka, A.; Turavets, U.; Hoha, A.; Salerno, M. Two-Level 3D Column-like Nanofilms with Hexagonally–Packed Tantalum Fabricated via Anodizing of Al/Nb and Al/Ta Layers—A Potential Nano-Optical Biosensor. *Materials* **2023**, *16*, 993. [CrossRef]
29. Butanovs, E.; Kuzmin, A.; Piskunov, S.; Smits, K.; Kalinko, A.; Polyakov, B. Synthesis and characterization of GaN/ReS_2, ZnS/ReS_2 and ZnO/ReS_2 core/shell nanowire heterostructures. *Appl. Surf. Sci.* **2021**, *536*, 147841. [CrossRef]
30. Rao, C.; Rao, G. *Transition Metal Oxides*; Department of Chemistry, Indian Institute of Technology: Kanpur, India, 1974.
31. Patnaik, P. *Handbook of Inorganic Chemicals*; McGraw-Hill: New York, NY, USA, 2003.
32. Li, P.; Stender, C.; Ringe, E.; Marks, L.D.; Odom, T.W. Synthesis of TaS_2 Nanotubes From Ta_2O_5 Nanotube Templates. *Small* **2010**, *6*, 1096–1099. [CrossRef]
33. Najafi, L.; Bellani, S.; Oropesa-Nuñez, R.; Martín-García, B.; Prato, M.; Pasquale, L.; Panda, J.K.; Marvan, P.; Sofer, Z.; Bonaccorso, F. TaS_2, $TaSe_2$, and Their Heterogeneous Films as Catalysts for the Hydrogen Evolution Reaction. *ACS Catal.* **2020**, *10*, 3313–3325. [CrossRef]
34. Sim, Y.; Chae, Y.; Kwon, S.Y. Recent advances in metallic transition metal dichalcogenides as electrocatalysts for hydrogen evolution reaction. *iScience* **2022**, *25*, 105098. [CrossRef]
35. Wang, M.; Zhang, L.; Huang, M.; Liu, Y.; Zhong, Y.; Pan, J.; Wang, Y.; Zhu, H. Morphology-controlled Tantalum Diselenide Structures as Self-optimizing Hydrogen Evolution Catalysts. *Energy Environ. Mater.* **2020**, *3*, 12–18. [CrossRef]
36. Doebelin, N.; Kleeberg, R. *Profex*: A graphical user interface for the Rietveld refinement program *BGMN*. *J. Appl. Crystallogr.* **2015**, *48*, 1573–1580. [CrossRef]
37. Ulrich, F.; Zachariasen, W.H. Ueber die kristallstruktur des alpha- und beta-CdS, sowie des wurtzits. *Z. Fur Krist.* **1925**, *62*, 260–273.
38. McMurdie, H.F.; Morris, M.C.; Evans, E.H.; Paretzkin, B.; Wong-Ng, W.; Ettlinger, L.; Hubbard, C.R. Standard X-Ray Diffraction Powder Patterns from the JCPDS Research Associateship. *Powder Diffr.* **1986**, *1*, 64–77. [CrossRef]
39. Moon, H.; Nam, C.; Kim, C.; Kim, B. Synthesis and photoluminescence of zinc sulfide nanowires by simple thermal chemical vapor deposition. *Mater. Res. Bull.* **2006**, *41*, 2013–2017. [CrossRef]
40. Aleshina, L.A.; Loginova, S.V. Rietveld analysis of X-ray diffraction pattern from β-Ta_2O_5 oxide. *Crystallogr. Rep.* **2002**, *47*, 415–419. [CrossRef]
41. Yang, Y.; Kawazoe, Y. Prediction of new ground-state crystal structure of Ta_2O_5. *Phys. Rev. Mater.* **2018**, *2*, 034602. [CrossRef]
42. Lawan Adam, M.; Buba Garba, I.; Alhaji Bala, A.; Aji Suleiman, A.; Muhammad Gana, S.; Lawan Adam, F. Tuning superconductivity and charge density wave order in $TaSe_2$ through Pt intercalation. *Phys. Rev. B* **2023**, *107*, 104510. [CrossRef]
43. Swanson, H.E.; Tatge, E. *Standard X-ray Diffraction Powder Patterns*; National Bureau of Standards (U.S.) Circular Nr. 539; National Bureau of Standards: Gaithersburg, MD, USA, 1953; Section I, 33.
44. Wyckoff, R.W.G. *Crystal Structures*, 2nd ed.; Interscience Publishers: New York, NY, USA, 1963; Volume 1.
45. Luo, H.; Xie, W.; Tao, J.; Pletikosic, I.; Valla, T.; Sahasrabudhe, G.S.; Osterhoudt, G.; Sutton, E.; Burch, K.S.; Seibel, E.M.; et al. Differences in Chemical Doping Matter: Superconductivity in $Ti_{1-x}Ta_xSe_2$ but Not in $Ti_{1-x}Nb_xSe_2$. *Chem. Mater.* **2016**, *28*, 1927–1931. [CrossRef]